Atmósfera 39, 283-295 (2025)
https://doi.org/10.20937/ATM.53446

New experimental device for measuring electrical charge of precipitation particles

Rodolfo Guillermo PEREYRA[1,2]*, Lucía Belén MARTÍNEZ[1,2] and Eldo Edgardo ÁVILA[1,2]

[1] *Facultad de Matemática, Astronomía, Física y Computación (FAMAF), Universidad Nacional de Córdoba (UNC), Av. Medina Allende s/n, Ciudad Universitaria, X5000HUA Córdoba, Argentina.*
[2] *Instituto de Física Enrique Gaviola (IFEG), CONICET, Av. Medina Allende s/n, Ciudad Universitaria, X5000HUA Córdoba, Argentina.*
*Corresponding author; email: rodolfo.pereyra@unc.edu.ar

Received: October 9, 2024; Accepted: February 4, 2025

RESUMEN

En este trabajo se presenta el nuevo diseño de un dispositivo para medir la carga eléctrica transportada por las partículas de precipitación y su correspondiente velocidad de caída. El instrumento representa una versión mejorada del anterior, con el objetivo principal de aumentar la tasa de muestreo de gotas cargadas, y mejorar y robustecer el análisis estadístico de las gotas de lluvia cargadas. Además, el instrumento incorpora un programa computacional para la detección de pasajes individuales de gotas de lluvia, lo que permite el cálculo automático tanto de la carga eléctrica como de la velocidad de caída de cada gota de lluvia. Para probar el rendimiento del nuevo dispositivo, se utilizó simultáneamente con el instrumento original durante una tormenta en Córdoba el 21 de noviembre de 2023. Se observó que el nuevo instrumento aumentó la tasa de muestreo casi cinco veces en comparación con el anterior. Los resultados muestran un alto grado de consistencia entre los diferentes dispositivos y validan la fiabilidad y reproducibilidad del nuevo aparato.

ABSTRACT

A new approach is presented in this work to measure the electrical charge carried by precipitation particles and their corresponding fall velocity. The instrument represents an improved version of our previous device, with the primary goal of increasing the sampling rate of charged droplets to improve and make the statistical analysis of charged raindrops more robust. Additionally, the instrument incorporates a computational program for detecting individual raindrop passages, enabling automatic calculation of its electrical charge and fall velocity. To test the new device's performance, it was simultaneously used with our previous instrument during a storm in Córdoba on November 21, 2023. It was observed that the latest instrument increased the sampling rate nearly fivefold compared to the old one. The results demonstrate a high degree of consistency across different devices, validating the reliability and reproducibility of the new device.

Keywords: thunderstorms, electrical charge measurements, charged raindrops, size of raindrops, Córdoba storm, fall velocity.

1. Introduction

In typical thunderstorms, precipitation particles carry electric charges, mainly acquired through collisions between distinct ice particles, such as hail, graupel, snow pellets, snowflakes, and ice crystals. The sign and magnitude of the charges acquired through this mechanism depend on the complex dynamic and microphysical processes within the cloud (Reynolds et al., 1957; Takahashi, 1978; Ávila et al., 1998; MacGorman and Rust, 1998; Saunders and Peck,

1998; Ávila and Pereyra, 2000; Pereyra and Ávila, 2002). Therefore, the charges carried by raindrops can be closely related to the distribution of charges in thunderstorms (Marshall and Stolzenburg, 1998; Medina et al., 2021; Ávila et al., 2022).

On the other hand, the electric charge on the droplets could be modified by the presence of ions or aerosols sited below the cloud. This is a consequence of the high polarizability of the water droplets that facilitates the capture of charged aerosols or ions near their surface. These charges and the presence of electrical forces can modify the capture process among water droplets, which, in turn, may affect the cloud microphysical processes and the precipitation mechanism (Khain et al., 2004; Harrison et al., 2015). The collision and coalescence processes between cloud droplets are crucial for broadening the droplet size distribution and facilitating precipitation development. Thus, the knowledge of the electric charges carried by raindrops is of great relevance and has been reported since the pioneering work of Gschwend (1921).

The operational principle of the experimental device used to measure the charge and size of precipitation particles was described by Gunn and Kinzer (1949) and is based on the electrical induction produced by the passage of charged droplets through metallic rings. Connecting the metallic rings to suitable charge amplifiers allows us to determine the charge carried by the raindrops. Concurrently, by measuring the time difference it takes to pass between two induction rings, it is possible to calculate the fall velocity of the droplets. Knowing the fall velocity allows to determine the droplet size. It is important to note that this technique requires prior calibration of the charge sensors to determine the actual magnitude of the charge.

Numerous works in the literature report measurements of charges and sizes of precipitation particles, among which we can mention: Gunn and Kinzer (1949), Gunn (1950), Gunn and Devin (1953), Chauzy and Despiau (1980), Weinheimer et al. (1991), Despiau and Houngninou (1996), Bateman et al. (1999), Mo et al. (2007), and Ávila et al. (2022). The conventional technique used by raindrop charge measuring instruments requires the passage of raindrops through two or more metal rings connected to electronic amplifiers; only raindrops that successfully traverse all the rings can be measured. However, it is common for rain to occur in the presence of horizontal winds, which can produce deviations of the raindrops' vertical falls that cause the drops to impact the rings or the wall supporting them. This effect can cause the loss of many droplets that cannot be recorded.

In order to improve the detection efficiency of charged raindrops and to make statistical analysis more robust, a new experimental device was designed, constructed, and presented in this work. The principle of its operation was based on expanding the cross-sectional angle for droplet capture. In addition to the new experimental device, software entirely designed to obtain information on the charge and size of each drop is presented.

2. Materials and methods

2.1 Measuring device

Figure 1a illustrates the experimental setup holding a 6 cm diameter, 1.5 cm long brass induction ring positioned 5.7 cm above a flat aluminum plate 20 cm diameter. Both the ring and plate are electrically connected to high-gain current amplifiers with an amplification of 5×10^8. To safeguard against electromagnetic interference, the ring, plate, and amplifiers are enclosed within a metal container (Faraday cage). Furthermore, the amplifiers are protected from potential water damage as they are secured within a waterproof enclosure. The Faraday cage features an opening slightly larger than the ring, enabling raindrops to enter solely through the induction ring. All water that reaches the plate is drained through its sides and collected in an aluminum container, which is also situated within the Faraday cage and electrically isolated from it.

The current inverter amplifier circuit is shown in Figure 1b. The two analog signals from the ring and plate amplifiers are processed at a digitization rate of 5 kHz per channel using an MC USB-1608FS-Plus data acquisition device and digitized via a desktop computer with LabVIEW software. A photo of the instrument is shown in Figure 1c.

As mentioned in the introduction, the aim was to facilitate the measurement of raindrops that exhibit notable deviation from a strictly vertical descent. This objective has been effectively achieved through the

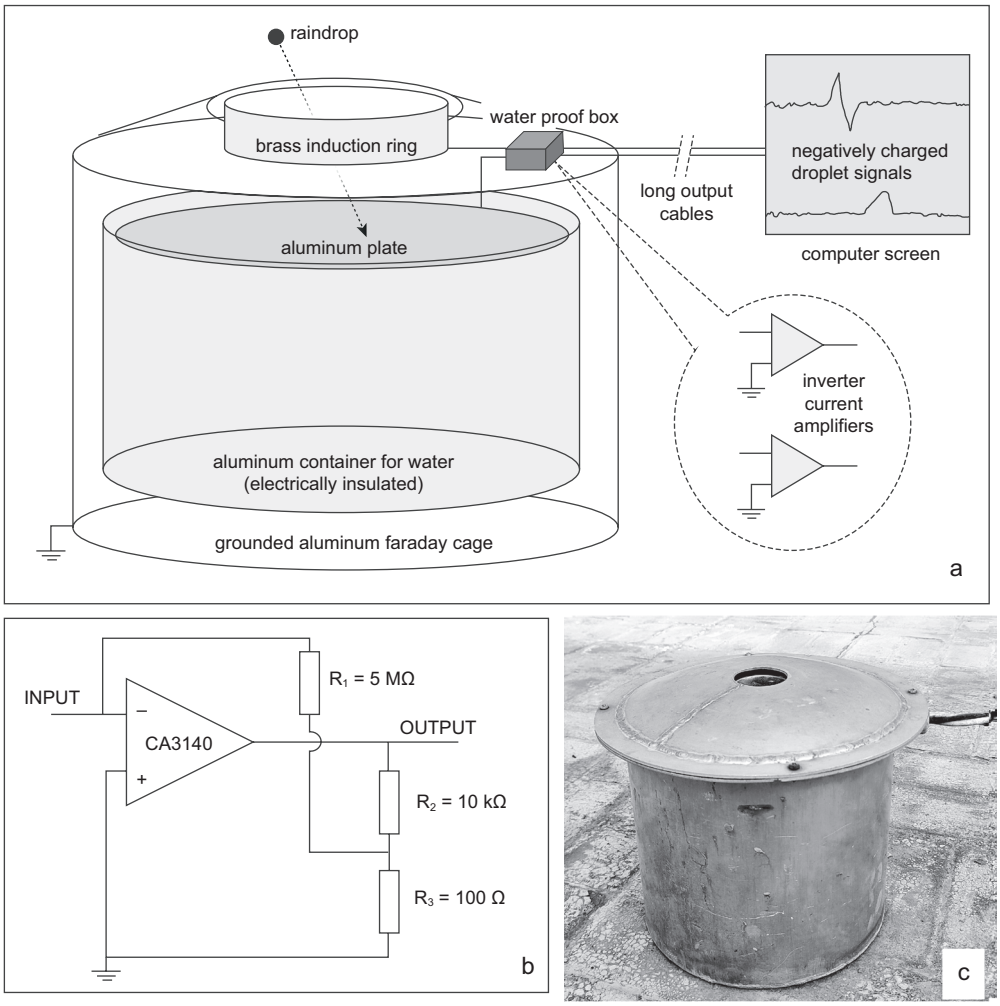

Fig. 1. (a) Diagram of the measuring device; (b) current inverter amplifier circuit; (c) photograph of the device on the roof of the Faculty of Mathematics, Astronomy, Physics, and Computing, National University of Cordoba.

innovative design we present. In Figure 2, another schematic diagram of the new device is depicted, emphasizing its distinctive attribute of featuring a significantly broader cross-sectional aperture angle, approximately 150°. This angle value comes from the height and diameter of the ring. The dotted lines in Fig. 2 represent the trajectories of the droplets with the highest angle, which are able to pass inside the ring without hitting it. This modification substantially enhances the probability of capturing raindrops. This advancement primarily arises from the ring's proximity to the apparatus inlet and its diminished height. These factors collectively facilitate the passage of raindrops that descend at steeper angles, enhancing the device's capability to detect electric charges.

Furthermore, the plate introduces an added advantage to the measurement process. The total charge on the plate is discharged through a resistor. By integrating the current flowing through the resistor, it is possible to determine the actual charge carried by the raindrop. To confirm that it is possible to determine the total charge of a raindrop using this method, auxiliary experiments were conducted in which droplets with known charges were impacted onto the plate. A dropper that produced charged droplets was used, with the droplets passing through induction rings

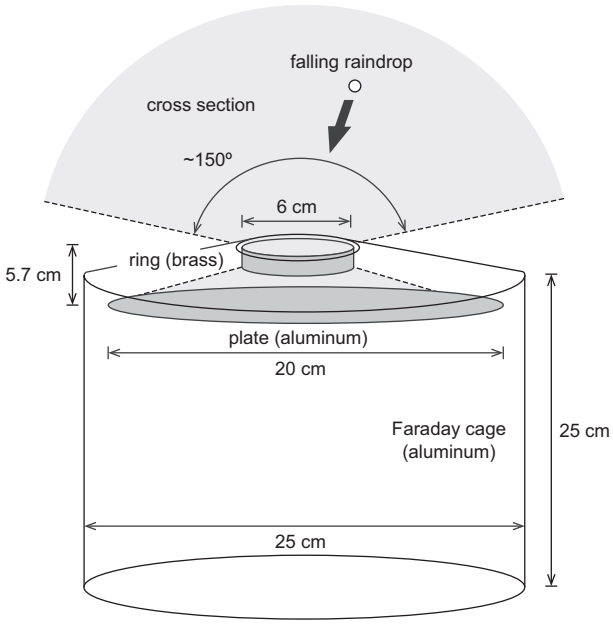

Fig. 2. Dimensions and cross-section of the experimental device's raindrop collection.

connected to previously calibrated charge amplifiers, a device employed in Ávila et al. (2022). In this way, the charge of each droplet impacting the plate was determined. A statistical analysis of 100 droplets with varying charge magnitudes and polarities revealed that the average difference between the charge determined by integrating the current and the charge measured using the calibrated induction rings was 4%, with a maximum observed difference of 7%.

The design parameters of the instrument were based on empirical knowledge acquired through various tests with several previous prototypes. The relevant dimensions of the instrument are the height and diameter of the ring, as well as the plate-ring distance. All other dimensions do not influence its operation.

The goal when designing the device was to detect the passage of raindrops falling at any angle relative to the vertical, which is theoretically achieved with a ring height as thin as possible. However, the technical constraint of fixing the ring in position set a limit to this height. Thus, the ring must have a minimum height of 1.5 cm.

The other key parameter is the ring diameter, which has to be as large as possible to increase the effective capture angle for raindrops. However, there are two practical limitations to enlarging the ring diameter. First, if the diameter ring is larger, the probability of signal overlaps due to multiple raindrop passages increases. Second, the detection sensitivity of the amplifier decreases because the electric charge induced on the ring by the passage of a charged drop is reduced. Thus, a ring diameter of 6 cm was selected.

Finally, the distance between the plate and the ring is a key parameter in determining the fall speed of raindrops. It was selected empirically at 5.7 cm because a larger separation increases the probability of signal overlaps due to multiple raindrop passages. A shorter separation makes it difficult to determine the difference in raindrop passage time between the ring and the plate.

2.2 Setting up the signals of the amplifiers

Due to computer limitations, the acquisition process cannot be performed simultaneously with data recording to the hard drive. The acquisition is suspended for approximately 50 ms every second to allow for writing the file, resulting in a loss of around 5% of the data. The signals present gaps with no information, as shown in Figure 3a. Both channels have a noise of approximately 0.02 V peak-to-peak, mounted on a line offset that can be any value between –0.5 and 0.5 V, depending on the current status of each amplifier. For example, in the case shown in Figure 3a, the ring channel has an offset of 0.12 V, and the plate channel has an offset of –0.07 V.

To perform further analysis, it is necessary to fill in the gaps with no data acquisition and remove the offsets of the signals from both channels. We use a Fortran program to add the missing rows, assigning a constant voltage to each channel. These constants are the average value of the signal of the 1000 points (0.2 s) before and after the gap. The modified signals are shown in Figure 3b. Subsequently, the offsets are eliminated by subtracting the centered simple moving average of 10 000 points (5000 on each side) from the signals. The resulting signals after this and a high-pass filter are shown in Figure 3c. The last step before the pulse search is the sign inversion of both signals since the current amplifiers are inverters.

2.3 Detection of charged raindrop pulses

Charged droplets near a metallic surface induce a charge on the surface. If the droplets are in motion,

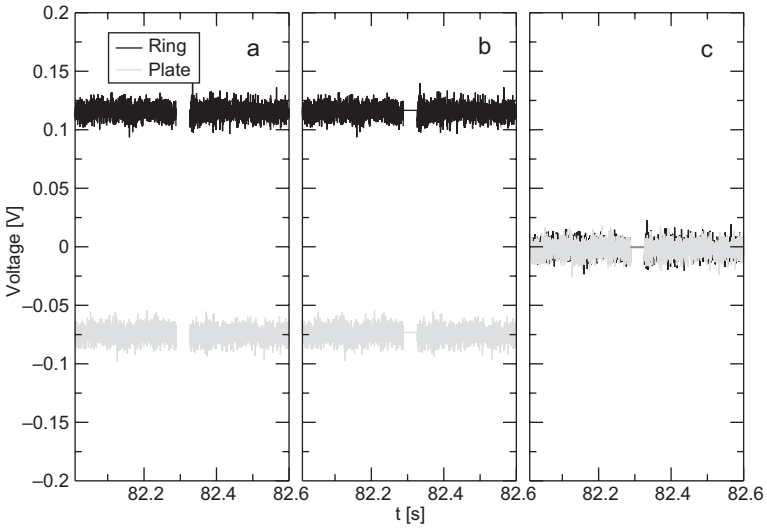

Fig. 3: Ring (black line) and plate (grey line) signals. (a) The original signals obtained from the data acquisition device; (b) the signal after gap-filling processing; and (c) the signal after applying a high-pass filter.

they generate an electric current due to the movement of the induced charges. When a charged droplet approaches the surface, it generates a current of a specific polarity, depending on the sign of the droplet's charge. Conversely, as the droplet moves away from the surface, the current reverses its polarity. Figure 4 displays the signal produced when a positively charged raindrop passes through the ring and hits the plate. In this device, charged raindrops can simultaneously induce an electric charge on the ring and the plate due to their proximity. The maximum induced current on the ring and the plate occurs when

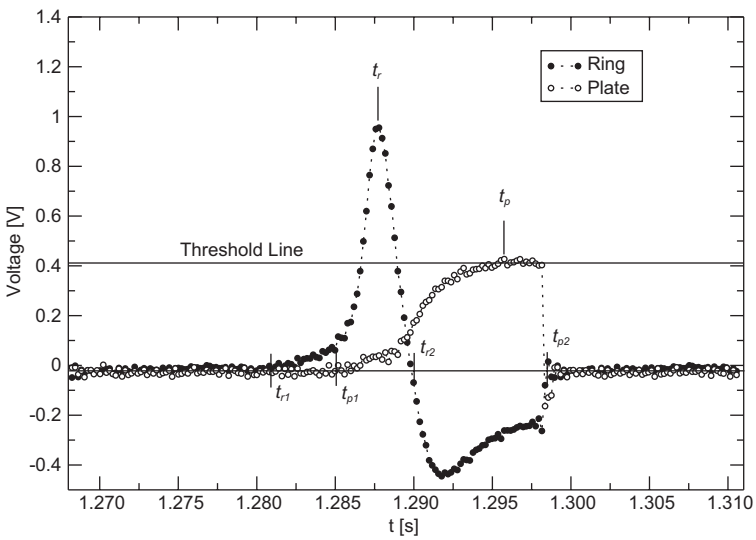

Fig. 4. Pulses of a positively charged raindrop passing through the ring (filled circles) and plate (hollow circles) sensors.

the raindrop is in the central region of the ring and on the surface of the plate, respectively. In this way, it is possible to determine the times when the raindrop passes through the center of the ring and when it impacts the plate. A negatively charged raindrop has a similar aspect but is reflected on the zero-volt line.

The device includes a new computational program designed to detect individual raindrop passages, enabling the automatic calculation of each raindrop's electrical charge and fall velocity. An algorithm is used to automatically identify these pulses. Essentially, this algorithm searches for the characteristic times of each pulse, i.e., the starting and ending points of pulses of the ring and plate. Below, we describe the procedure followed to search for positive pulses (similarly for negative pulses).

First, the algorithm involves scanning the data file to identify pairs of "peaks" in the signals, one from the ring and another from the plate amplifiers, which correspond to the passage of raindrops. We defined a peak as a portion of the signal where at least two points exceed or equal a threshold value. The time assigned to a peak is the corresponding time of the point with the maximum value, which are named t_r and t_p, respectively (see Fig. 4, where the threshold value is 0.41 V).

To identify a raindrop, the algorithm looks for pairs of peaks in the ring and plate signals that are temporally separated by no more than 0.02 seconds (100 points). If a ring pulse peak occurs before a plate pulse peak and the temporal separation between them satisfies the maximum interval criterion, they are considered as corresponding to the same raindrop. In summary: it must happen that $t_r < t_p$ and $t_p - t_r \leq 0.02$ s.

The procedure for detecting the pair of peaks in all raindrop pulses involves scanning the ring and plate signals 2000 times. A threshold value is established during each scan, and the peaks corresponding to the charged droplets are searched for. The threshold value starts at 2 V in the first scan and progressively decreases to 0.02 V by the last scan.

Once the two peaks of a droplet are identified, the algorithm determines the two "limit" times for each pulse. The ring pulse's left and right limit times are denoted by t_{r1} and t_{r2}, while those for the plate pulse are denoted by t_{p1} and t_{p2}. The locations of these four limit times are shown in Figure 4. The information between these pairs of times is used to calculate the charge of the raindrop, as explained in the next section.

After each scan is finished, the data from t_{r1} and t_{p2}, for all identified drops, is saved in an auxiliary file and zeroed in the principal file to prevent re-detection in subsequent scans with lower thresholds. By the end of the 2000 scans, the algorithm has identified the pulses of all possible charged raindrops, as the final threshold value (0.02 V) is close to the level of electrical noise, making it impossible to detect any more raindrops. Subsequent calculations are performed exclusively on the data saved in the auxiliary file.

2.4 Electrical charge and fall velocity of raindrops

The electrical charges detected by the ring and plate are calculated by integrating the pulse voltage from t_{r1} to t_{r2} and t_{p1} to t_{p2}, respectively. This involves summing all voltage values between these two limits. Figure 5 shows the integrated pulses from Figure 4. To convert the time-integrated voltage to charge units, it is necessary to multiply by 4×10^{-13}, which means that 1 V corresponds to 0.4 pC. This proportionality factor is obtained from the inverse of the product of 5×10^8 and 5×10^3, which are the amplification factor and the sampling rate, respectively. Although we obtain two different charge values, q_r and q_p, corresponding to the ring and plate sensors, respectively, these numbers correspond to only one raindrop. Therefore, we must obtain a single value for this quantity. We assign the weighted arithmetic mean of these two measurements as the electrical charge (q) of the raindrop, which is calculated using the following equation (Eq. 1):

$$q = \frac{q_r w_r + q_p w_p}{2} \tag{1}$$

The weights for q_r and q_p are denoted as w_r and w_p, respectively. After conducting supplementary calibration measurements, which involved releasing water droplets through a dropper, allowing them to pass through the center of the ring and then impact the plate, it was observed that the droplets exiting the dropper carried a random charge sign and magnitude. A statistical analysis of 500 drops determined that the value detected by the ring was 0.87 ± 0.05 times the value detected by the plate. As a result, we use the values $w_r = 1/0.87$ and $w_p = 1$ as the weights for the ring and plate electrodes, respectively. In the example

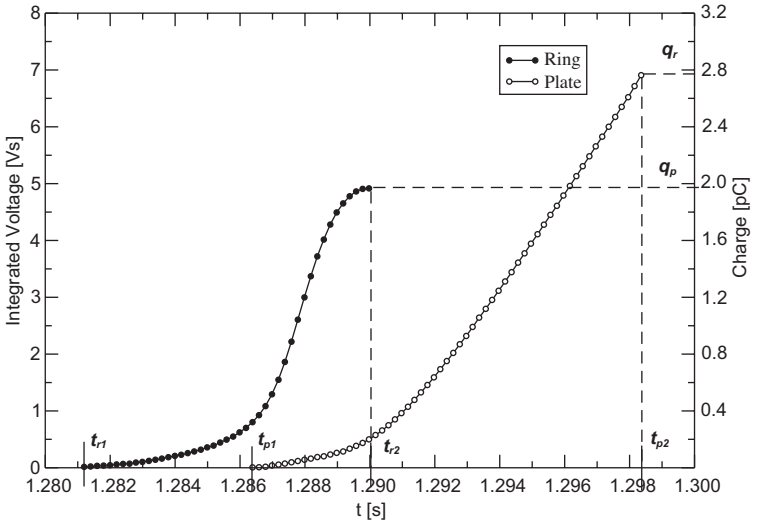

Fig. 5. Pulses integrated from t_{r1} to t_{r2}, and from t_{p1} to t_{p2} for the ring (filled circles) and plate (hollow circles) signals, respectively.

in Figure 5, the charges are $q_r = 1.97$ pC and $q_p = 2.76$ pC, resulting in a value of $q = 2.51$ pC.

To determine the fall velocity, v, of a raindrop, we divide the ring-plate distance, $d = 0.057$ m by the time between t_{r2} to t_{p2}. The t_{r2} corresponds to the point at which the raindrop crosses the central plane of the ring, and t_{p2} corresponds to the time that the drop hits the plate. The equation (Eq. 2) used to calculate the velocity is:

$$v = \frac{d}{t_{p2} - t_{r2}} \tag{2}$$

In the case of the example shown in Figure 4, the times are $t_{r2} = 1.2900$ s and $t_{p2} = 1.2986$ s, giving a value of $v = 6.6$ m s^{-1}. Each measurement is determined with an uncertainty of 0.4 ms, resulting in a time difference uncertainty of 0.8 ms. Considering that the ring-plate distance has an uncertainty of 1 mm, error propagation analysis indicates that the fall velocity can be determined with an uncertainty of 9 and 15% for velocities of 5 and 9 m s^{-1}, respectively.

However, not all pairs of pulses that meet the conditions mentioned above correspond to a raindrop. Overlapping pulses from different raindrops can cause confusion and incorrect assignments. To reduce the number of invalid counts, the algorithm has a filter that eliminates situations that do not correspond to the passage of a raindrop. The filter imposes conditions on both the electrical charge (q_r and q_p) and the fall velocity of the raindrops. The conditions for the charges are:

1. $|q_r| \geq 0.3$ pC and $|q_p| \geq 0.3$ pC
2. The charges q_r and q_p must have the same sign.
3. $0.5 \leq q_r/q_p \leq 2$. That is, neither of the two charges should be more than twice the other.
4. 0.5 m s$^{-1} \leq v \leq 9$ m s^{-1}

To obtain the diameters of the charged raindrops, we use a semi-empirical formula given in Beard (1976), which examines the terminal velocity as a function of the raindrop diameter (D) for different flow regimes, as shown in Figure 6. However, it is important to note that this function cannot be inverted directly. Therefore, we employ an algorithm to find the corresponding diameter D_0 for a given velocity v_0. We utilize the numerical bisection method to search for the root of the equation $v(D) - v_0$, ensuring a precision of one decimal place. For the case depicted in Figure 4, with a velocity of 6.6 m s^{-1}, the corresponding diameter is 2.0 mm.

Considering the uncertainty in determining each velocity, droplets with diameters of 2 mm and 3 mm are estimated to have uncertainties of 20 and 30%, respectively. The uncertainties increase for larger droplets because the velocities of droplets larger than 3 mm tend to approach a constant value, as shown in

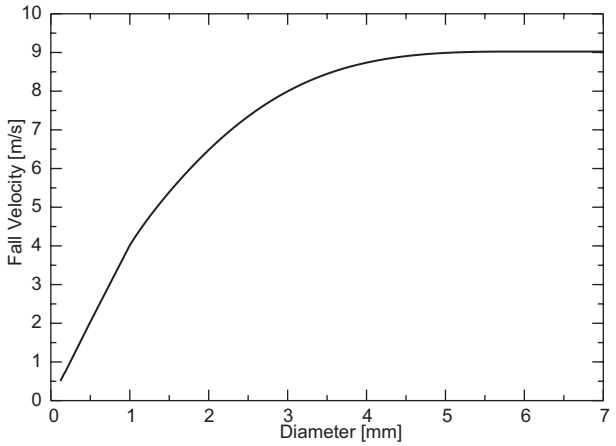

Fig. 6. Fall velocity as a function of raindrop diameter according to Beard (1976).

Figure 6. Therefore, we conclude that this method is suitable for determining the sizes of raindrops up to 3 mm in diameter.

3. Results

3.1. New device's performance

To test the performance of the new device, the charge and size of the raindrops were measured during a storm in Córdoba City, Argentina. The current experimental device was used simultaneously with the device employed by Ávila et al. (2022). In this way, it was possible to directly verify whether there was an improvement in the efficiency of charged droplet detection.

Two new devices with different amplifications were constructed to expand the range of detectable charges. The first one, D1, has a gain of 5×10^8 and can measure charges in the range of –50 to +50 pC (this device was described in the previous section); the second device, D2, is similar to D1 but has a gain of 1×10^8, enabling it to measure charges within the range of –250 to +250 pC (in this device $R_1 = 1$ MΩ, see Fig. 1b).

3.2 Description of the storm

The measurement of charged raindrops from the storm on November 21, 2023, occurred from 17:46 to 18:27 UTC. Figure 7a shows the brightness temperature over Córdoba measured by the GOES-16 satellite, using a color scale. This corresponds to 17:40 UTC, 6 min before the observation of charged drops began. The geographical location of Córdoba is marked by a point and a black arrow. Figure 7b presents the electrical activity over Córdoba, detected by the GLM lightning sensor aboard GOES-16. This corresponds to 17:40 UTC, when the maximum number of discharges was observed 10 min after the minimum cloud-top temperature was reached. Each blue point in Figure 7b represents an observed discharge. In Figure 7c, the temporal evolution of the brightness temperature measured over Córdoba is shown for the period from 16:30 UTC to 18:50 UTC, encompassing the timeframe during which charged raindrops were measured. The red and green circles represent the approximate start and end times of the measurement of the charged drop, respectively. Meanwhile, the yellow circle indicates when the cloud reached its minimum temperature during the measurement period. The temperature decreases over time, reaching its minimum brightness temperature at 17:30 UTC, approximately 16 min before the start of the charged drop measurement at 17:46 UTC. After reaching the minimum brightness temperature and the start of the measurement, the temperature gradually rises over time, indicating the storm dissipation over Córdoba, with the measurement ending at 18:27 UTC.

3.3 Results of electrical charge and size of raindrops

Figure 8 depicts the temporal evolution of the charges measured by each instrument. Figure 8a displays the measured charge by the new instrument with maximum amplification (D1), where each point represents the individual charges of the measured droplets, and the black line indicates the average charges over 10-min intervals. Figure 8b illustrates the measured charge with the device with lower amplification (D2), and Figure 8c shows the measured charges with the induction ring system (IR) utilized in previous studies (Ávila et al., 2022).

The number of charged raindrops detected by D1 was 2034, D2 recorded 1007 raindrops, and the IR system detected 441 raindrops. It can be observed that the new devices (D1 and D2) detected charged droplets throughout the entire rainfall, whereas induction rings detected a limited number of charged droplets after 2500 seconds from the start of the measurement. This coincides with a significant surface wind that

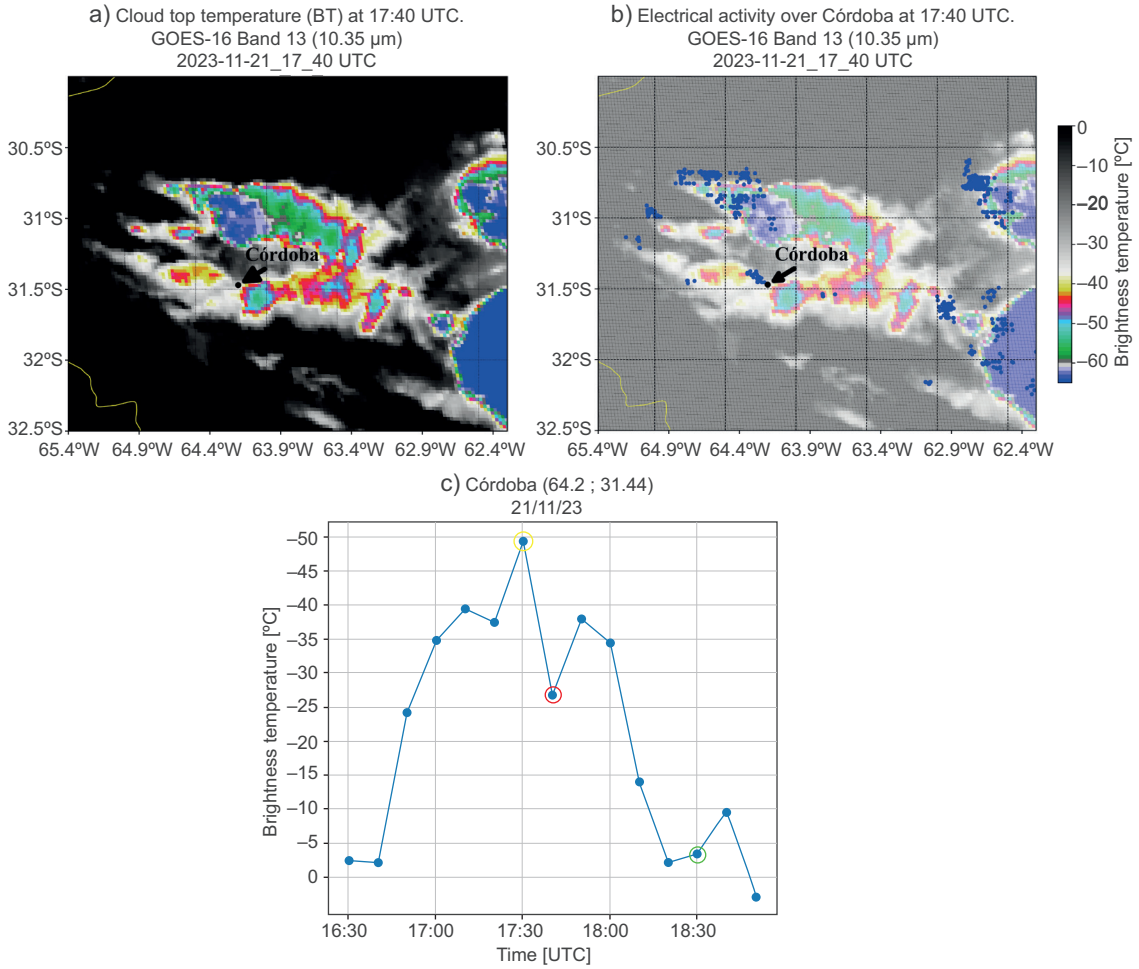

Fig. 7. (a) Satellite image of the cloud top at 17:40 UTC, close to the start of the storm measurement on November 23, 2021. (b) Maximum detected electrical activity by GOES-GLM over Córdoba at 17:40 UTC. (c) Temporal evolution of brightness temperature during the charged droplet measurement period. The yellow circle marks the moment when the cloud reached its minimum temperature during this period, and the red and green circles indicate the approximate start and end times of the charged droplet measurement, respectively.

began to blow afterward. It was observed that over 80% of the charges detected by D1 have magnitudes less than 5 pC. Because most raindrops carry small charges, D1, having five times higher gain than D2, detects larger number of charged raindrops than D2 (approximately a factor of 2).

Figure 9 displays the curves of the averaged charges for each device. The observed trend is very similar for all three devices. The IR shows a higher charge average than the other two devices, while D1 presents the lowest charge averages obtained.

The charge magnitudes for the droplets measured by all three devices range from –20 to 40 pC. Figure 10 presents the histograms of charges for each device. As mentioned earlier, D1 detects a larger number of raindrops than D2, particularly more droplets with small charges, while D2 detects a few droplets with larger charges that D1 does not detect. These results indicate that D1 effectively covers the complete range of charge magnitudes. Due to its higher gain in detecting droplets with small charges, it records the highest number of events, resulting in lower average charge values.

Regarding the size of charged raindrops, it can be observed that all three devices report similar results. Figure 11 displays the temporal evolution of the

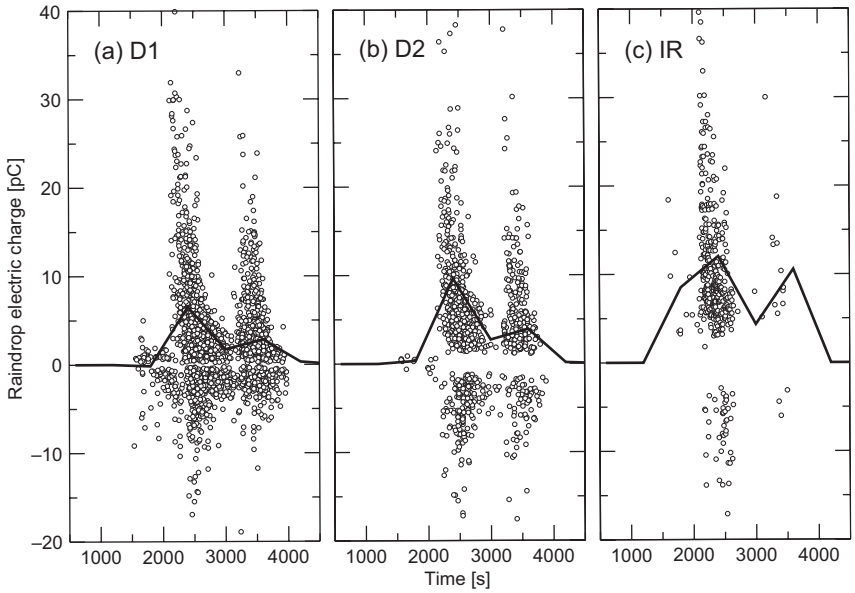

Fig. 8. Electrical charges of all raindrops detected by D1, D2, and IR devices, plotted against the occurrence time (zero seconds correspond to the start time of the record). The grey hollow circles represent the individual charge per raindrop, and the thick black line depicts the average charge every 10 min.

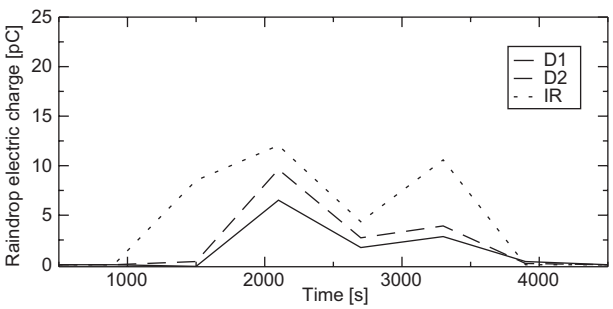

Fig. 9. Comparison of the 10-min averaged charges among the three devices: D1 (continuous line), D2 (segmented line) and IR (dotted line).

averaged droplet diameters obtained in 10-min intervals. Both the trends of the curves and the average values are similar across the measurements.

In summary, the new device demonstrates improved performance in measuring the charge and size of raindrops. The results indicate that the proposed experimental setup effectively achieves its intended objective of improving the sampling rate of charged raindrops.

4. Summary and conclusions

In this study, we have introduced a new device designed to measure the fall velocity and electric charge carried by precipitation particles during storms. The instrument was developed by redesigning our previous device, with the main objective of enhancing the detection of the number of charged droplets. This enhancement was essential to ensure more accurate and reliable statistical analysis of charged raindrops in future studies, allowing for deeper insights into their behavior, distribution, and potential impact on atmospheric electrical phenomena.

The device incorporates a computational program that detects individual raindrop passages, enabling the automatic calculation of every raindrop's electrical charge and fall velocity. This is very useful, as it allows us to have the data available for storm analysis shortly after it occurs.

A measurement of charged droplets was conducted during a storm, comparing the efficiency of the newly presented device with the device used in Ávila et al. (2022). The increase in droplets obtained by the new instrument for the same measurement is

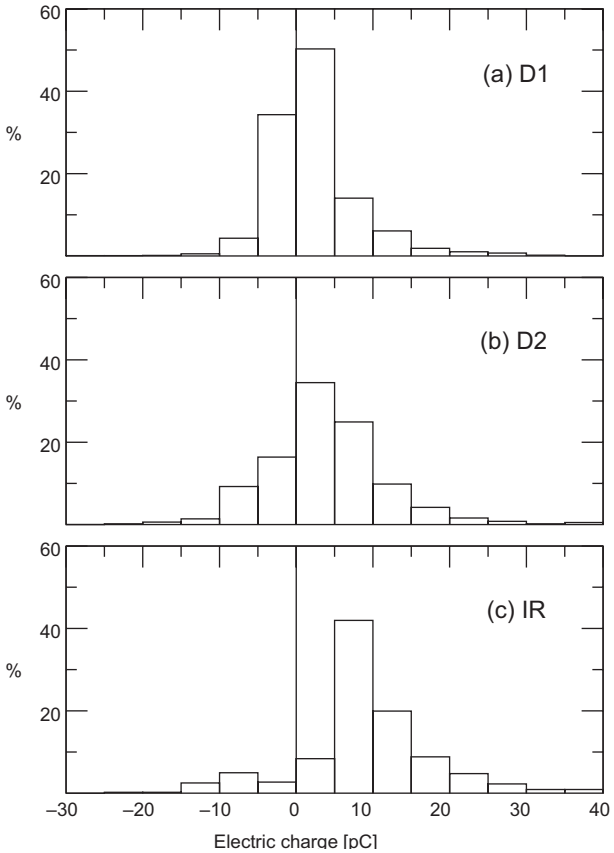

Fig. 10. Histograms of electric charges calculated in 5 pC bins for each of the (a) D1, (b) D2, and (c) IR devices.

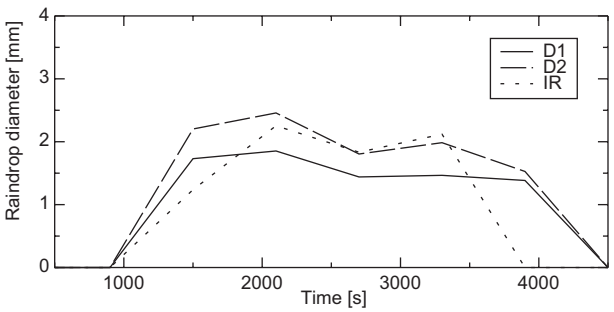

Fig. 11. Comparison of the 10-min averaged diameter of the raindrops detected by each device.

confirmed. The number of droplets detected by the two new devices created was five times (D1) and two times (D2) more than the IR device. The range of charges for the measured droplets across the three devices was very similar. The results of these measurements allow us to verify an improvement in the efficiency of detecting charged droplets compared to the former device.

By increasing the sampling rate of charged droplets, this instrument enables us to measure a larger number of charged droplets during storm development. This allows us to rigorously correlate the temporal sequence of charged droplets reaching the surface with the possible charge structures in storms within the detection region. Besides, by measuring the temporal evolution of charged droplets reaching the surface at various sites, it will be possible to analyze how the electrical structures of storms vary at each observation site.

This instrument will also be used to study the correlation between discharges occurring during storms and the sizes and charges of raindrops reaching the surface. By analyzing variations in the sizes, charges, and concentrations of raindrops as a consequence

of these discharges, it will be possible to study the phenomenon of abrupt increases in precipitation intensity shortly after a nearby lightning strike, which has often been observed in thunderstorms.

On the other hand, with improved counting efficiency of charged raindrops, this device can be useful for determining changes in the precipitation current flux at the surface, which is closely related to variations in the surface electric field. Simultaneous measurements of precipitation current and electric field are highly relevant for understanding the end of storm oscillation (EOSO) effect (Pawar and Kamra, 2007).

Acknowledgments

This work was supported by the Secretaría de Ciencia y Tecnología of the Universidad Nacional de Córdoba (SECYT-UNC), Consejo Nacional de Investigaciones Científicas y Tecnológicas (CONICET), and Agencia Nacional de Promoción Científica y Tecnológica (FONCYT).

References

Ávila E, Caranti G, Castellano N, Saunders C. 1998. Laboratory studies of the influence of cloud droplet size on charge transfer during crystal-graupel collisions. Journal of Geophysical Research: Atmospheres 103: 8985-8996. https://doi.org/10.1029/97JD03115

Ávila EA, Pereyra RG. 2000. Charge transfer during crystal-graupel collisions for two different cloud droplet size distributions. Geophysical Research Letters 27: 3837-3840. https://doi.org/10.1029/2000GL012302

Ávila E, Martínez L, Pereyra R, Lang T, Deierling W, Wingo M, Melo G, Medina B. 2022. Measurements of size and electrical charges carried by precipitation particles during RELAMPAGO field campaign. Earth and Space Science 9: e2022EA002407. https://doi.org/10.1029/2022EA002407

Bateman MG, Marshall TC, Stolzenburg M, Rust WD. 1999. Precipitation charge and size measurements inside a New Mexico mountain thunderstorm. Journal of Geophysical Research Atmospheres 104: 9643-9653. https://doi.org/10.1029/1998JD200118

Beard KV. 1976. Terminal velocity and shape of cloud and precipitation drops aloft. Journal of the Atmospheric Sciences 33: 851-864. https://doi.org/10.1175/1520-0469(1976)033<0851:TVASOC>2.0.CO;2

Chauzy S, Despiau S. 1980. Rainfall rate and electric charge and size of raindrops of six spring showers. Journal of the Atmospheric Sciences 37: 1619-1627. https://doi.org/10.1175/1520-0469(1980)037<1619:RRAECA>2.0.CO;2

Despiau S, Houngninou E. 1996. Raindrop charge, precipitation, and Maxwell currents under tropical storms and showers. Journal of Geophysical Research Atmospheres 101: 14991-14997. https://doi.org/10.1029/95JD03657

Gschwend, P. 1921. Beobachtungen über die elektrischen Ladungen einzelner Regentropfen und Schneeflocken. Jahrbuch der Radioaktivität und Elektronik 17: 62-79.

Gunn R, Kinzer GD. 1949. The terminal velocity of fall for water droplets in stagnant air. Journal of the Atmospheric Sciences 6: 243-248. https://doi.org/10.1175/1520-0469(1949)006<0243:TTVOFF>2.0.CO;2

Gunn R. 1950. The free electrical charge on precipitation inside an active thunderstorm. Journal of Geophysical Research (1896-1977) 55: 171-178. https://doi.org/10.1029/JZ055i002p00171

Gunn R, Devin C. 1953. Raindrop charge and electric field in active thunderstorms. Journal of the Atmospheric Sciences 10: 279-284. https://doi.org/10.1175/1520-0469(1953)010<0279:RCAEFI>2.0.CO;2

Harrison RG, Nicoll KA, Ambaum MHP. 2015. On the microphysical effects of observed cloud edge charging. Quarterly Journal of the Royal Meteorological Society 141: 2690-2699. https://doi.org/10.1002/qj.2554

Khain A, Arkhipov V, Pinsky M, Feldman Y, Ryabov Y. 2004. Rain enhancement and fog elimination by seeding with charged droplets. Part I: Theory and numerical simulations. Journal of Applied Meteorology and Climatology 43: 1513-1529. https://doi.org/10.1175/JAM2131.1

MacGorman DR, Rust WD. 1998. The electrical nature of storms. Oxford University Press. https://doi.org/10.5860/choice.36-1028

Marshall TC, Stolzenburg M. 1998. Estimates of cloud charge densities in thunderstorms. Journal of Geophysical Research Atmospheres 103: 19769-19775. https://doi.org/10.1029/98JD01674

Medina BL, Carey LD, Lang TJ, Bitzer PM, Deierling W, Zhu Y. 2021. Characterizing charge structure in central

Argentina thunderstorms during RELAMPAGO utilizing a new charge layer polarity identification method. Earth and Space Science 8: e2021EA001803. https://doi.org/10.1029/2021EA001803

Mo Q, Detwiler AG, Helsdon J, Winn WP, Aulich G, Murray WC. 2007. Hydrometeor charges observed below an electrified cloud using a new instrument. Journal of Geophysical Research: Atmospheres 112: D13207. https://doi.org/10.1029/2006JD007809

Pawar SD, Kamra AK. 2007. End-of-storm oscillation in tropical air mass thunderstorms. Journal of Geophysical Research Atmospheres 112: D03204. https://doi.org/10.1029/2005JD006997

Pereyra RG, Ávila EE. 2002. Charge transfer measurements during single ice crystal collisions with a target growing by riming. Journal of Geophysical Research: Atmospheres 107: AAC 23-1-AAC 23-9. https://doi.org/10.1029/2001JD001279

Reynolds SE, Brook M, Gourley MF. 1957. Thunderstorm charge separation. Journal of the Atmospheric Sciences 14: 426-436. https://doi.org/10.1175/1520-0469(1957)014<0426:tcs>2.0.co;2

Saunders CPR, Peck SL. 1998. Laboratory studies of the influence of the rime accretion rate on charge transfer during crystal/graupel collisions. Journal of Geophysical Research: Atmospheres 103: 13949-13956. https://doi.org/10.1029/97JD02644

Takahashi T. 1978. Riming electrification as a charge generation mechanism in thunderstorms. Journal of the Atmospheric Sciences 35: 1536-1548. https://doi.org/10.1175/1520-0469(1978)035<1536:REAACG>2.0.CO;2

Weinheimer AJ, Dye JE, Breed DW, Spowart MP, Parrish JL, Hoglin TL, Marshall TC. 1991. Simultaneous measurements of the charge, size, and shape of hydrometeors in an electrified cloud. Journal of Geophysical Research Atmospheres 96: 20809-20829. https://doi.org/10.1029/91JD02262